The Astrophysical Journal, submitted
Preprint typeset using LaTeX style emulateapj v. 6/22/04

arXiv:astro-ph/0501227v2 26 May 2005

EFFECTS OF COOLING AND STAR FORMATION ON THE BARYON FRACTIONS IN CLUSTERS

Andrey V. Kravtsov[1,2,3], Daisuke Nagai[1,3], Alexey A. Vikhlinin[4,5]

The Astrophysical Journal, submitted

ABSTRACT

We study the effects of radiative cooling and galaxy formation on the baryon fractions in clusters using high-resolution cosmological simulations that resolve formation of cluster galaxies. The simulations of nine individual clusters spanning a decade in mass are performed with the shock-capturing eulerian adaptive mesh refinement N-body+gasdynamics ART code. For each cluster the simulations were done in the adiabatic regime (without dissipation) and with radiative cooling and several physical processes critical to various aspects of galaxy formation: star formation, metal enrichment and stellar feedback. We show that radiative cooling of gas and associated star formation increase the total baryon fractions within radii as large as the virial radius. The effect is strongest within cluster cores, where the simulations with cooling have baryon fractions larger than the universal value, in contrast to the adiabatic simulations in which the fraction of baryons is substantially smaller than universal. At larger radii ($r \gtrsim r_{500}$) the cumulative baryon fractions in simulations with cooling are close to the universal value. The *gas* fractions in simulations with dissipation are reduced by $\approx 20-40\%$ at $r < 0.3r_{\rm vir}$ and $\approx 10\%$ at larger radii compared to the adiabatic runs, because a fraction of gas is converted into stars. There is an indication that gas fractions within different radii increase with increasing cluster mass as $f_{\rm gas} \propto M_{\rm vir}^{0.2}$. We find that the total baryon fraction within the cluster virial radius does not evolve with time in both adiabatic simulations and in simulations with cooling. The gas fractions in the latter decrease slightly from $z=1$ to $z=0$ due to ongoing star formation.

Finally, to evaluate systematic uncertainties in the baryon fraction in cosmological simulations we present a comparison of gas fractions in our adiabatic simulations to re-simulations of the same objects with the entropy-conserving SPH code Gadget. The cumulative gas fraction profiles in the two sets of simulations on average agree to better than $\approx 3\%$ outside the cluster core ($r/r_{\rm vir} \gtrsim 0.2$), but differ by up to 10% at small radii. The differences are smaller than those found in previous comparisons of eulerian and SPH simulations. Nevertheless, they are systematic and have to be kept in mind when using gas fractions from cosmological simulations.

Subject headings: cosmology: theory–clusters: formation– methods: numerical

1. INTRODUCTION

In hierarchical models of structure formation clusters of galaxies form via collapse of a large representative volume and are therefore expected to contain the baryons and dark matter in proportions close to the universal average. This fact together with independent measurements of the universal baryon fraction can be used as a powerful constraint on the mean density of matter in the universe (e.g., White et al. 1993; Evrard 1997). The apparent evolution of baryon fraction with redshift can be used to put constraints on the energy density content of the universe and properties of dark energy (Sasaki 1996; Pen 1997). The universality of cluster baryon fractions can be used to estimate total cluster mass and construct mass functions of clusters at different redshifts (Vikhlinin et al. 2003).

Recently, deep X-ray observations of nearby and high-redshift clusters have been used to measure the cluster baryon fraction and constrain the power spectrum shape and normalization (Voevodkin & Vikhlinin 2004), the matter and dark energy density of the universe (Allen et al. 2002, 2004; Vikhlinin et al. 2003; Chen & Ratra 2004), and even the neutrino mass and the equation of state of dark energy (Allen et al. 2004). Sunyaev-Zeldovich (SZ) effect observations combined with X-ray observations have also been used to measure the cluster baryon fraction and constrain the matter energy density of the universe (Grego et al. 2001). These measurements are complementary to (and competitive with) cosmological constraints using supernovae type Ia and anisotropies of the cosmic microwave background and are likely to be improved. However, they rely on the key assumptions that the baryon fraction within a given radius can be measured reliably, is independent of redshift, and can be converted to the universal fraction by the correction factor derived from cosmological simulations.

In order to improve the baryon fraction based cosmological constraints and to better understand associated systematic uncertainties, these assumptions have to be carefully tested with simulations. During the last decade, a number of studies have considered the cluster baryon fraction and its evolution in cosmological simulations in the adiabatic regime (i.e., without radiative cooling). The main results of these stud-

---

[1] Department of Astronomy and Astrophysics, Kavli Institute for Cosmological Physics, 5640 South Ellis Ave., The University of Chicago, Chicago, IL 60637

[2] The Enrico Fermi Institute, The University of Chicago, Chicago, IL 60637

[3] `daisuke,andrey@oddjob.uchicago.edu`

[4] Harvard-Smithsonian Center for Astrophysics, 60 Garden Street, Cambridge, MA 02138

[5] Space Research Institute, 8432 Profsojuznaya St., GSP-7, Moscow 117997, Russia

ies are: (1) the baryon fraction within the cluster virial radius evolves only very weakly with time and (2) is in general $\approx 10-15\%$ lower than the universal average (Evrard 1990; Metzler & Evrard 1994; Navarro et al. 1995; Lubin et al. 1996; Eke et al. 1998; Frenk et al. 1999; Mohr et al. 1999; Bialek et al. 2001); (3) this "baryon depletion" can be enhanced by strong pre-heating of gas (Bialek et al. 2001; Borgani et al. 2002; Muanwong et al. 2002; Kay et al. 2003). Note, however, that high-resolution eulerian simulations of Anninos & Norman (1996) exhibit baryon fraction larger than universal. Moreover, systematic comparison of adiabatic simulations of a massive cluster performed with different numerical codes (Frenk et al. 1999) has revealed systematic differences. The eulerian shock-capturing codes have generally produced clusters with little or no "baryon depletion," while gas fractions in SPH simulations were $\approx 10\%$ below the universal value. This indicates that there are systematic differences in gas and dark matter density profiles in simulations done with different numerical schemes.

More recently, several groups have presented analysis of baryon fractions in simulations that include gas cooling and star formation (Muanwong et al. 2002; Kay et al. 2003; Valdarnini 2003; Ettori et al. 2004). These simulations have shown that cooling can increase the total baryon fraction (gas + stars) and change its dependence on cluster mass and cluster-centric radius compared to the adiabatic simulations.

The purpose of the present paper is twofold. First, given the systematic differences between numerical codes identified in Frenk et al. (1999), we would like to present a systematic study of the cluster baryon fractions in eulerian adaptive mesh refinement (AMR) simulations and compare them to the results obtained with modern SPH codes. Second, we investigate the effects of radiative cooling and star formation on the baryon fractions in the very high-resolution AMR simulations that resolve formation of individual cluster galaxies.

The paper is organized as follows. In § 2 we describe our simulations and implementation of radiative cooling and star formation. In § 3 we compare gas fraction profiles in our adiabatic simulations with the simulations of the same clusters performed with the entropy-conserving Gadget code. In § 4 we discuss convergence tests and assess effects of resolution. In § 5 we present our main results and compare them to the previous results in § 6. Finally, in § 7 we discuss our conclusions and implications of the presented results for cluster observations and their use as cosmological probes.

2. SIMULATIONS

In this study, we analyze high-resolution cosmological simulations of nine cluster-size systems in the "concordance" flat ΛCDM model: $\Omega_{\rm m} = 1 - \Omega_\Lambda = 0.3$, $\Omega_{\rm b} = 0.04286$, $h = 0.7$ and $\sigma_8 = 0.9$, where the Hubble constant is defined as $100h$ km s^{-1} Mpc^{-1}, and σ_8 is the power spectrum normalization on $8h^{-1}$ Mpc scale. The simulations were done with the Adaptive Refinement Tree (ART) N-body+gasdynamics code (Kravtsov 1999; Kravtsov et al. 2002), a Eulerian code that uses adaptive refinement in space and time, and (non-adaptive) refinement in mass (Klypin et al. 2001) to reach the high dynamic range required to resolve cores of halos formed in self-consistent cosmological simulations.

To set up initial conditions we first ran a low resolution simulation of $80h^{-1}$ Mpc and $120h^{-1}$ Mpc boxes and selected nine clusters with the virial masses ranging from $\approx 7\times10^{13}$ to $8.2\times10^{14}h^{-1}$ M$_\odot$. The properties of clusters at the present epoch are listed in Table 1. The perturbation modes in the lagrangian region corresponding to the sphere of several virial radii around each cluster at $z = 0$ was then re-sampled at the initial redshift, $z_i = 49$ for eight clusters and $z_i = 25$ for the most massive cluster in the sample. For the Coma-size cluster we have resampled radius of $1.5R_{\rm vir}(z = 0)$, while for the rest of the clusters the resampling sphere had radius of $5R_{\rm vir}$. During the resampling we retained the previous large-scale waves intact but included additional small-scale waves, as described by Klypin et al. (2001). The resampled lagrangian region of each cluster was then re-simulated with high dynamic range.

High-resolution simulations were run using 128^3 uniform grid and 8 levels of mesh refinement in the computational boxes of $80h^{-1}$ Mpc for CL2-CL9 and $120h^{-1}$ Mpc for the Coma-size CL1, which corresponds to the dynamic range of $128\times2^8 = 32768$ and peak formal resolution of $80/32,768 \approx 2.44h^{-1}$ kpc, corresponding to the actual resolution of $\approx 2\times2.44 \approx 5h^{-1}$ kpc. Only the region of $\sim 3-10h^{-1}$ Mpc around the cluster was adaptively refined, the rest of the volume was followed on the uniform 128^3 grid. The mass resolution corresponds to the effective 512^3 particles in the entire box, or the Nyquist wavelength of $\lambda_{\rm Ny} = 0.469h^{-1}$ and $0.312h^{-1}$ *comoving* megaparsec for CL1 and CL2-9, respectively, or $0.018h^{-1}$ and $0.006h^{-1}$ Mpc in the physical units at the initial redshift of the simulations. The dark matter particle mass in the region around the cluster was $2.7\times10^8h^{-1}$ M$_\odot$ for CL2-CL9 and $9.1\times10^8h^{-1}$ M$_\odot$ for CL1, while other regions were simulated with lower mass resolution.

As the zeroth-level fixed grid consisted of only 128^3 cells, we started the simulation already pre-refined to the 2nd level ($l = 0, 1, 2$) in the high-resolution lagrangian regions of clusters. This is done to ensure that the cell size is equal to the mean interparticle separation and all fluctuations present in the initial conditions are evolved properly. During the simulation, the refinements were allowed to the maximum $l = 8$ level and refinement criteria were based on the local mass of DM and gas in each cell. The logic is to keep the mass per cell approximately constant so that the refinements are introduced to follow the collapse of matter in a quasi-lagrangian fashion. For the DM, we refine the cell if it contains more than two dark matter particles of the highest mass resolution specie. For gas, we allow the mesh refinement, if the cell contains gas mass larger than four times the DM particle mass scaled by the baryon fraction. In other words, the mesh is refined if the cell contains the DM mass larger than $2(1-f_b)m_p$ or the gas mass larger than $= 4f_bm_p$ (where m_p is given above and $f_b = \Omega_{\rm b}/\Omega_{\rm m} = 0.1429$). We analyze clusters at the present-day epoch as well as their progenitors at higher redshifts.

We repeated each cluster simulation with and without radiative cooling. The first set of "adiabatic" simulations have included only the standard gasdynamics for the baryonic component without dissipation and star formation. The second set of simulations included gasdynamics

TABLE 1
SIMULATED CLUSTER SAMPLE AT $z = 0$

Name	$R_{\rm vir}$ h^{-1}Mpc	$M_{\rm vir}$	$M_{\rm 180m}$	$M_{\rm 200c}$ $10^{14}h^{-1}$ $\mathrm{M}_\odot$	$M_{\rm 500c}$	$M_{\rm 2500c}$	$\langle T_{\rm X}^{\rm ad}\rangle$ keV	$\langle T_{\rm X}^{\rm csf}\rangle$ keV
CL1	1.911	8.21	9.62	6.73	5.31	2.78	6.9	8.6
CL2	1.205	2.06	2.32	1.75	1.34	0.75	2.7	2.6
CL3	1.227	2.17	2.45	1.87	1.32	0.69	2.7	3.8
CL4	1.187	1.97	2.37	1.65	1.24	0.63	2.8	3.2
CL5	1.016	1.23	1.41	1.01	0.78	0.39	1.8	1.7
CL6	0.906	0.87	0.99	0.78	0.62	0.34	1.6	2.5
CL7	0.947	1.00	1.22	0.66	0.48	0.24	1.4	1.0
CL8	0.966	1.06	1.24	0.88	0.65	0.34	1.7	2.1
CL9	0.795	0.59	0.68	0.51	0.35	0.13	0.8	1.2

and several physical processes critical to various aspects of galaxy formation: star formation, metal enrichment and thermal feedback due to the supernovae type II and type Ia, self-consistent advection of metals, metallicity dependent radiative cooling and UV heating due to cosmological ionizing background (Haardt & Madau 1996). We will use labels 'ad' and 'csf' for the adiabatic simulations and simulations with cooling and star formation, respectively. The cooling and heating rates take into account Compton heating and cooling of plasma, UV heating, atomic and molecular cooling and are tabulated for the temperature range $10^2 < T < 10^9$ K and a grid of metallicities, and UV intensities using the `Cloudy` code (ver. 96b4, Ferland et al. 1998). The Cloudy cooling and heating rates take into account metallicity of the gas, which is calculated self-consistently in the simulation, so that the local cooling rates depend on the local metallicity of the gas.

Star formation in these simulations was done using the observationally-motivated recipe (e.g., Kennicutt 1998): $\dot{\rho}_* = \rho_{\rm gas}^{1.5}/t_*$, with $t_* = 4\times10^9$ yrs. Stars are allowed to form in regions with temperature $T < 2\times10^4$ K and gas density $n > 0.1$ cm^{-3}. No other criteria (like the collapse condition $\nabla\cdot\mathbf{v} < 0$) are used. We have compared runs where star formation was allowed to proceed in regions different from our fiducial runs. We considered thresholds for star formation of $n = 10$, 1, 0.1, and 0.01 cm^{-3}. We find that thresholds affects gas fractions at small radii, $r/r_{\rm vir} < 0.1$, but the differences are negligible at the radii we consider in this study. The effect on the baryon fractions is small at all radii.

Algorithmically, star formation events are assumed to occur once every global time step $\Delta t_0 \sim 10^7$ yrs, the value close to the observed star formation timescales (e.g., Hartmann 2002). Collisionless stellar particles with mass $m_* = \dot{\rho}_*\Delta t_0$ are formed in every unrefined mesh cell that satisfies criteria for star formation during star formation events. The mass of stellar particles is restricted to be larger than $\min(5\times10^7 h^{-1}$ M$_\odot, 2/3\times m_{\rm gas})$, where $m_{\rm gas}$ is gas mass in the star forming cell. This is done in order to keep the number of stellar particles computationally tractable, while avoiding sudden dramatic decrease of the local gas density. In the simulations analyzed here, the masses of stellar particles formed by this algorithm range from $\approx 10^5$ to $7\times10^8 h^{-1}$ M$_\odot$.

Once formed, each stellar particle is treated as a single-age stellar population and its feedback on the surrounding gas is implemented accordingly. The feedback here is meant in a broad sense and includes injection of energy and heavy elements (metals) via stellar winds and supernovae and secular mass loss. Specifically, in the simulations analyzed here, we assumed that stellar initial mass function (IMF) is described by the Miller & Scalo (1979) functional form with stellar masses in the range $0.1 - 100$ M$_\odot$. All stars more massive than $M_* > 8$ M$_\odot$ deposit 2×10^{51} ergs of thermal energy in their parent cell[6] and fraction $f_{\rm Z} = \min(0.2, 0.01M_* - 0.06)$ of their mass as metals, which crudely approximates the results of Woosley & Weaver (1995). In addition, stellar particles return a fraction of their mass and metals to the surrounding gas at a secular rate $\dot{m}_{\rm loss} = m_*\, C_0(t - t_{\rm birth} + T_0)^{-1}$ with $C_0 = 0.05$ and $T_0 = 5$ Myr (Jungwiert et al. 2001). The code also accounts for the SNIa feedback assuming a rate that slowly increases with time and broadly peaks at the population age of 1 Gyr. We assume that a fraction of 1.5×10^{-2} of mass in stars between 3 and 8 M$_\odot$ explodes as SNIa over the entire population history and each SNIa dumps 2×10^{51} ergs of thermal energy and ejects 1.3 M$_\odot$ of metals into the parent cell. For the assumed IMF, 75 SNII (instantly) and 11 SNIa (over several billion years) are produced by a 10^4 M$_\odot$ stellar particle.

Throughout this paper we use estimates of gas and baryon fractions within different commonly used radii, defined by the total matter overdensity they enclose. We will use radii r_{2500}, r_{500}, r_{200} enclosing overdensities of 2500, 500, and 200 with respect to the critical density, $\rho_{\rm crit}$, as well as radii r_{180} and $r_{\rm vir}$ enclosing overdensities of 180 and $\Delta_{\rm vir}$ with respect to the mean density of the universe. The latter is equal to $\Delta_{\rm vir} \approx 334$ at $z = 0$ and ≈ 200 at $z = 1$ for the cosmology adopted in our simulations.

The virial radius and masses of clusters within different radii are given in Table 1. For reference, we also give average emission-weighted temperature in the radial range between 80 kpc to r_{500} of each cluster in adiabatic and cooling runs. The temperature is calculated as an

---

[6] No delay of cooling was introduced in these cells after SN energy release.

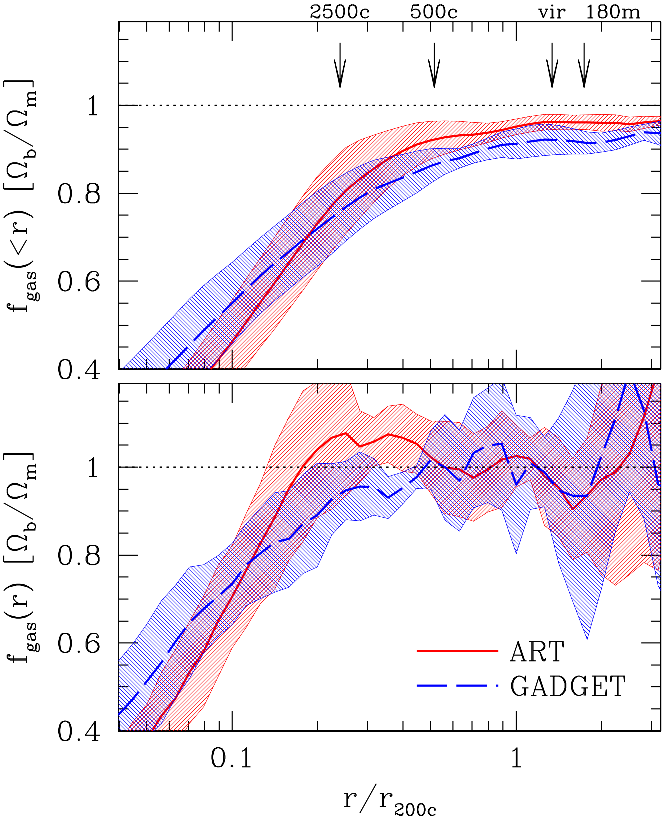

FIG. 1.— Comparison of the baryon fraction profiles in the adiabatic simulations of the eight clusters CL2-9 done with the ART (*solid lines*) and entropy-conserving Gadget (*long-dashed lines*) codes. The gas fractions are normalized to the universal baryon fraction of each simulation, while radii of all clusters are normalized to their respective radius enclosing the overdensity of 200 with respect to the critical density. The *bottom panel* shows differential gas fraction profiles, while the *top panel* shows corresponding cumulative profiles. The shaded bands represent 1σ *rms* scatter around the mean for the eight clusters. The vertical arrows in the top panel show the radii enclosing overdensities of 2500, 500 (with respect to $\rho_{\rm crit}$), the virial overdensity and the overdensity of 180 with respect to the mean density.

emission-weighted average convolved with the *Chandra* energy response in the 0.5−7 keV energy band.

3. COMPARISON OF THE ART AND GADGET SIMULATIONS

Before we begin, it is important to discuss the degree of numerical uncertainty in the baryon fractions derived from cosmological simulations. We will compare simulations of eight lower-mass clusters (CL2-CL9) from the Table 1 performed with the eulerian AMR Adaptive Refinement Tree code and the entropy conserving SPH Gadget code (Springel et al. 2001; Springel & Hernquist 2002) performed in the adiabatic regime. The ART simulations are described above, while the Gadget simulations are described by Ascasibar et al. (2003). We compare the CL2-CL9 for which the SPH simulations are available. In each case the simulations have been started from the identical initial conditions and ran in the same cosmology with comparable spatial and mass resolutions, although Gadget simulations used somewhat different values of $\Omega_{\rm b}$ for each individual cluster simulation. The number of dark matter particles is the same in the ART and Gadget simulations, while the number of gas particles varies but is of order million for all clusters. Both gravitational and the minimum SPH softening are in the range $\epsilon = 2-5h^{-1}$ kpc, depending on the number of particles within the virial radius.

The average cumulative and differential gas profiles in the two sets of simulations are compared in Figure 1. The figure shows a rather remarkable agreement (to a couple percent) in the differential profiles at $r \gtrsim 0.4r_{\rm vir}$, while at smaller radii there are systematic differences. The gas fraction profiles in the Gadget simulations are more centrally concentrated at $r < 0.2r_{\rm vir}$ compared to the ART simulations. At the same time, the gas fraction is systematically higher in the ART simulations at $r \sim 0.2-0.4r_{\rm vir}$. Comparison of the cumulative gas fraction profiles shows that despite the fact that the ART profiles are less centrally concentrated at small radii, the gas fraction within $0.4r_{\rm vir}$ is higher than in the Gadget simulations by $\approx 5\%$. At larger radii, $r \gtrsim r_{2500c}$, the systematic difference persists, although it is only about 3−5%. Note also that the scatter about the mean is similar in the ART and Gadget simulations. We checked that the differences in the mean profiles of the eight clusters also exist between profiles of individual clusters. They are therefore systematic and statistically significant.

The difference is significantly smaller than the systematic difference in gas fractions of $\approx 10\%$ between the eulerian and SPH codes, observed in the Santa Barbara cluster comparison project (Frenk et al. 1999). Indeed, agreement in gas and dark matter density profiles at this level is quite remarkable. Nevertheless, it is important to keep these systematic differences in mind, both in gauging implications of the results presented below and in observational analyses of gas fractions for cosmological constraints. As we argue below, this systematic difference is smaller than the uncertainty in the simulations with cooling and star formation, associated with the uncertain fraction of baryons in stars.

4. EFFECTS OF RESOLUTION

Given that in these simulations we are trying to resolve galaxy formation on kiloparsec scales while following formation of clusters self-consistently on scales of megaparsecs, it is reasonable to ask how the finite dynamic range of the simulations affects our results. To this end, we have re-run one of the clusters used in our study (CL3) with higher resolution. The re-simulations use more agressive refinement criteria, which results in a factor of $\simeq 2.5$ more refinement cells and a factor of two higher spatial resolution compared to the run used in this study. For example, the higher-resolution simulations at $z = 0$ has $\approx 2\times10^6$ grid cells on the 9th refinement level (comoving cell size of $1.22h^{-1}$ kpc), while the runs used in this study did not have refinement cells beyond the 8th level. Gas fraction profile in the adiabatic re-simulation with such higher resolution agrees with the lower resolution simulation to within $\simeq 1\%$ at all resolved radii. We find a similarly small difference for the higher-resolution re-simulation of this cluster with the Gadget code with eight times more particles and softening of $0.5h^{-1}$ kpc (compared to the $2-5h^{-1}$ kpc in the simulations we use for comparison). In other words, it appears that for each code convergence in adiabatic runs is reached, so that different resolution does not explain systematic differences in the gas fraction profiles discussed above.

The higher-resolution re-simulation of CL3 with cooling and star formation results in total baryon fraction profile that is within $\simeq 1-2\%$ of that in the low-resolution simulation. However, we find that the gas fraction is $\simeq 3-5\%$ higher in the higher resolution run. It is not clear what causes the difference, although we think that it is most likely be due to the increased heating by stellar feedback in the higher-resolution simulation. The difference is relatively small and is considerably smaller than the magnitude of the effects we discuss. Nevertheless, the effects of resolution in the runs with star formation will have to be studied further with higher-resolution runs.

5. RESULTS

We will start discussion of our results by considering an example of a single typical cluster from our sample (CL3). The cluster has virial mass similar to that of the Virgo cluster and has experienced a nearly equal-mass major merger at $z \approx 0.6$. We have analyzed three simulations of this cluster started from the same initial conditions but run including different physical processes. The first run was done in the "adiabatic" regime without radiative gas cooling and star formation. The second run included cooling and star formation. The third run is identical to the second at $z > 2$. At $z < 2$, however, gas dissipation and star formation have been artificially turned off. This run should be considered not as a realistic cluster model, but as a useful intermediate case between adiabatic run and run with full dissipation. For example, the fraction of baryons turned into stars within the virial radius is $f_* = 0.35$ in the simulation with cooling and $f_* = 0.15$ in the simulation with no cooling at $z < 2$ ($f_* = 0$ for the adiabatic simulation).

Figure 2 shows the cumulative and differential profiles of baryon and gas fraction for the three re-simulations of CL3. The figure shows several key qualitative effects of dissipation. The most salient difference is in the gas fraction. The simulation with cooling has the largest stellar fraction and, correspondingly, the smallest $f_{\rm gas}(< r_{\rm vir})$. The difference in cumulative gas fraction is approximately constant at $r \gtrsim 0.15 r_{\rm vir}$. However, the lower panel of Figure 2 shows that the difference in differential profile of $f_{\rm gas}$ increases monotonically with decreasing radius from less than 10% at $r \gtrsim 0.4 r_{\rm vir}$ to $\sim 30-40\%$ at smaller radii. This is because the central cluster galaxy has a significant effect on the overall stellar fraction and cumulative profile.

Comparison of the total baryon fraction profiles for the three runs reveals additional differences. The baryon fraction in the adiabatic simulation is significantly smaller than the universal value at $r \lesssim 0.2 r_{\rm vir}$, while it is larger than universal in the simulations with cooling. The cumulative baryon fraction in the adiabatic simulation reaches the universal value well beyond the virial radius. In the simulations with cooling the baryon fraction is close to the universal at the virial radius. Note that in all three runs the baryon fractions are within 10% of the universal value at $r \gtrsim 0.4 r_{\rm vir}$. The baryon fraction profiles are similar in all three simulations outside the virial radius.

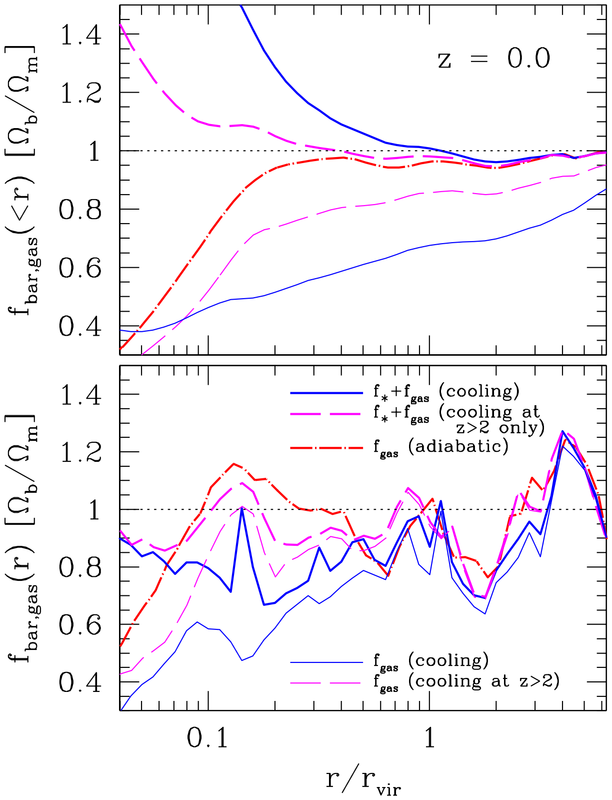

FIG. 2.— Effects of cooling on the cluster baryon and gas fraction profiles at $z = 0$. The figure shows profiles for the three resimulations of the Virgo-size cluster CL3. *Top panel:* the cumulative baryon and gas fractions within a given radius in the simulations with cooling (*solid*, *thick lines* show $f_{\rm gas} + f_*$ while *thin lines* show $f_{\rm gas}$), cooling only at $z > 2$ (*long-dashed lines*), and no cooling (or adiabatic, *dot-dashed line*). The radius is in units of the virial radius, defined as the radius enclosing overdensity of $\Delta_{\rm vir} = 334$ with respect to the mean density of the universe. The fractions are in units of the universal baryon fraction, Ω_b/Ω_m. *Bottom panel:* the same as the top panel, but for the differential profiles.

The main conclusion from this comparison, which also applies to the comparison of the mean profiles presented below, is that the cooling and star formation change not only the amplitude but also the shape of the gas and baryon fraction profiles in the simulated clusters.

This is to be expected because cooling and star formation lead to redistribution of both baryons and dark matter. The gas condensation results in a contraction of the dark matter halo (e.g., Zeldovich et al. 1980; Blumenthal et al. 1986) and steepening of the DM density profile at $r \lesssim 0.1 r_{\rm vir}$ (Gnedin et al. 2004). More significantly, dissipation and resulting star formation convert a fraction of gas into stars with the efficiency which may depend on the cluster radius. Dynamically, the stellar component is collisionless and its evolution will differ from that of the gas. For instance, cluster galaxies may loose their gas via ram pressure stripping. The lost gas can then mix with the intracluster gas at large radii. The stellar components of galaxies, on the other hand, can sink to the center via dynamical friction and build up the massive central cluster galaxy. Likewise, the detailed dynamics and relaxation process of gas and stars during mergers is rather different. For example, the gas experiences heating via shocks, while stars participate in collisionless violent relaxation.

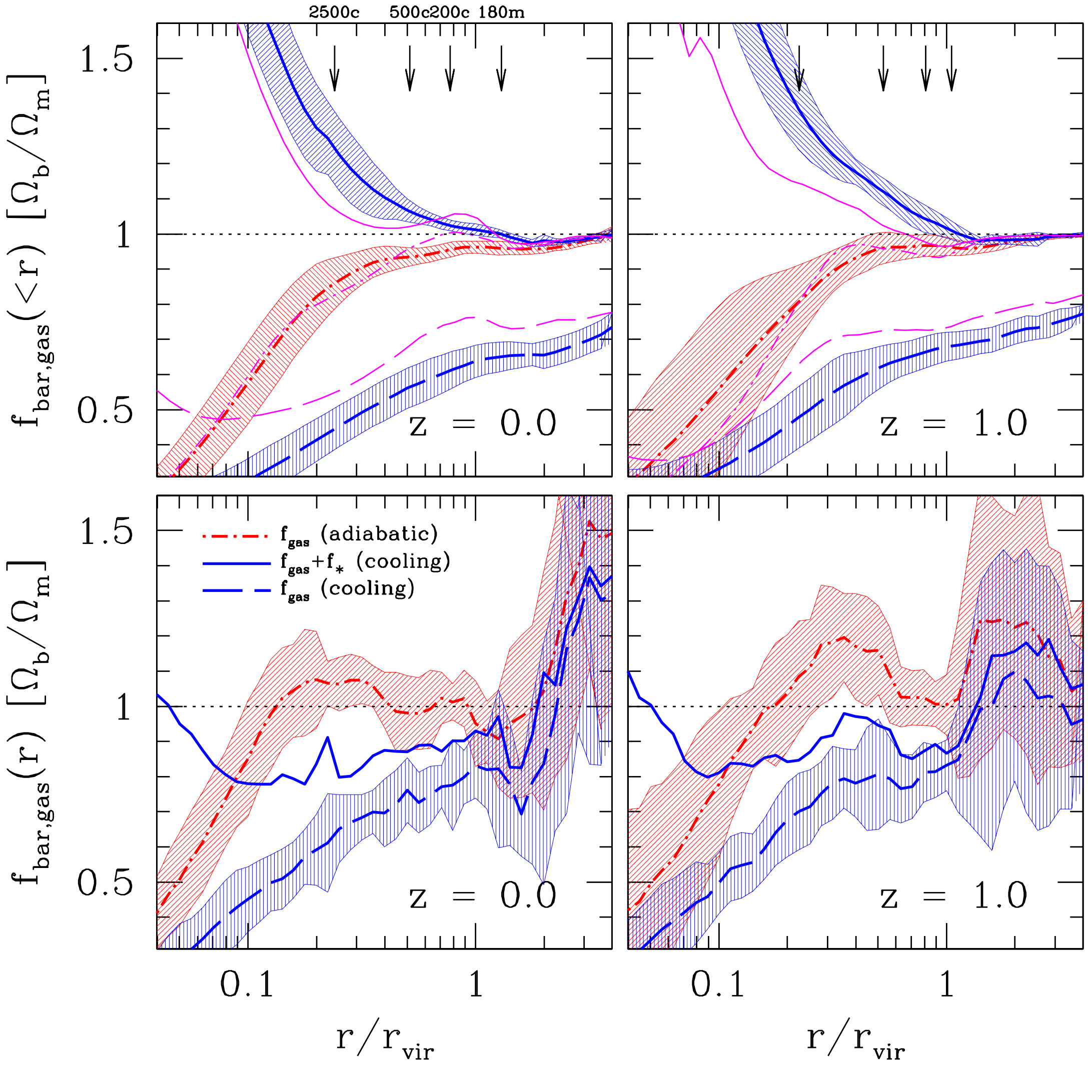

FIG. 3.— Differential (*bottom panels*) and cumulative (*top panels*) baryon and gas fraction profiles for the nine clusters used in our analysis at $z = 0$ (*left column*) and $z = 1$ (*right column*). The *dot-dashed* lines show the mean profiles in the adiabatic simulations averaged over eight clusters (CL2-CL9). The *solid* lines show the total mean baryon fraction (gas+stars) profile, while the *long-dashed* lines show the gas fraction profile in the simulations with cooling and star formation. The shaded bands show the 1σ *rms* scatter around the mean for the eight clusters. The *thin lines* in the top panels show the corresponding profiles in the Coma-size cluster simulation (CL1). These profiles have not been used in the averages due to systematically different gas and baryon fractions. The vertical arrows in the top panels show the radii enclosing overdensities of 2500, 500, 200 (with respect to $\rho_{\rm crit}$), and the overdensity of 180 with respect to the mean density.

Figure 3 shows the comparison of the mean baryon and gas fraction profiles at $z = 1$ and $z = 0$ for our entire sample of clusters simulated in the adiabatic regime and with dissipation. The profile for the Coma-size cluster (CL1) is plotted separately because in this cluster stellar fraction (and hence the gas fraction) is significantly different from the rest of the smaller-mass clusters, as we discuss below. However, the difference is mainly in the amplitude of the profile. Qualitatively, the profiles of CL1 are similar to the mean profile for the other eight clusters.

The trends in the mean profiles are similar to those seen in Figure 2. The cumulative baryon fraction profiles are flat at $r \gtrsim 0.4r_{\rm vir}$. At these radii $f_{\rm bar}$ is within $\approx 5\%$ of the universal value for both adiabatic and CSF runs, although in the former the $f_{\rm bar}$ is systematically below the universal value, while in the latter it is systematically above. In the cores of the low-mass clusters, the cumulative baryon fraction is considerably below (above) the universal value in the adiabatic (CSF) runs. This shows that dissipation and star formation result in a substantial redistribution of baryons within the virial radius. In the Coma-size cluster the baryon fraction is still close to the universal value within r_{2500}, but at smaller radii the trends are similar. Note that the differential baryon fraction in the CSF simulations is systematically below the universal value by $\approx 10-20\%$. The profile, however, is rather flat at $r \gtrsim r_{2500}$. Both the cumulative and differential gas fractions increase monotonically with radius. If a similar trend exists in real clusters this implies that the correction of gas fraction for stars in general depends on the cluster-centric radius and a single assumed value of f_* for all radii may not give the universal baryon fraction.

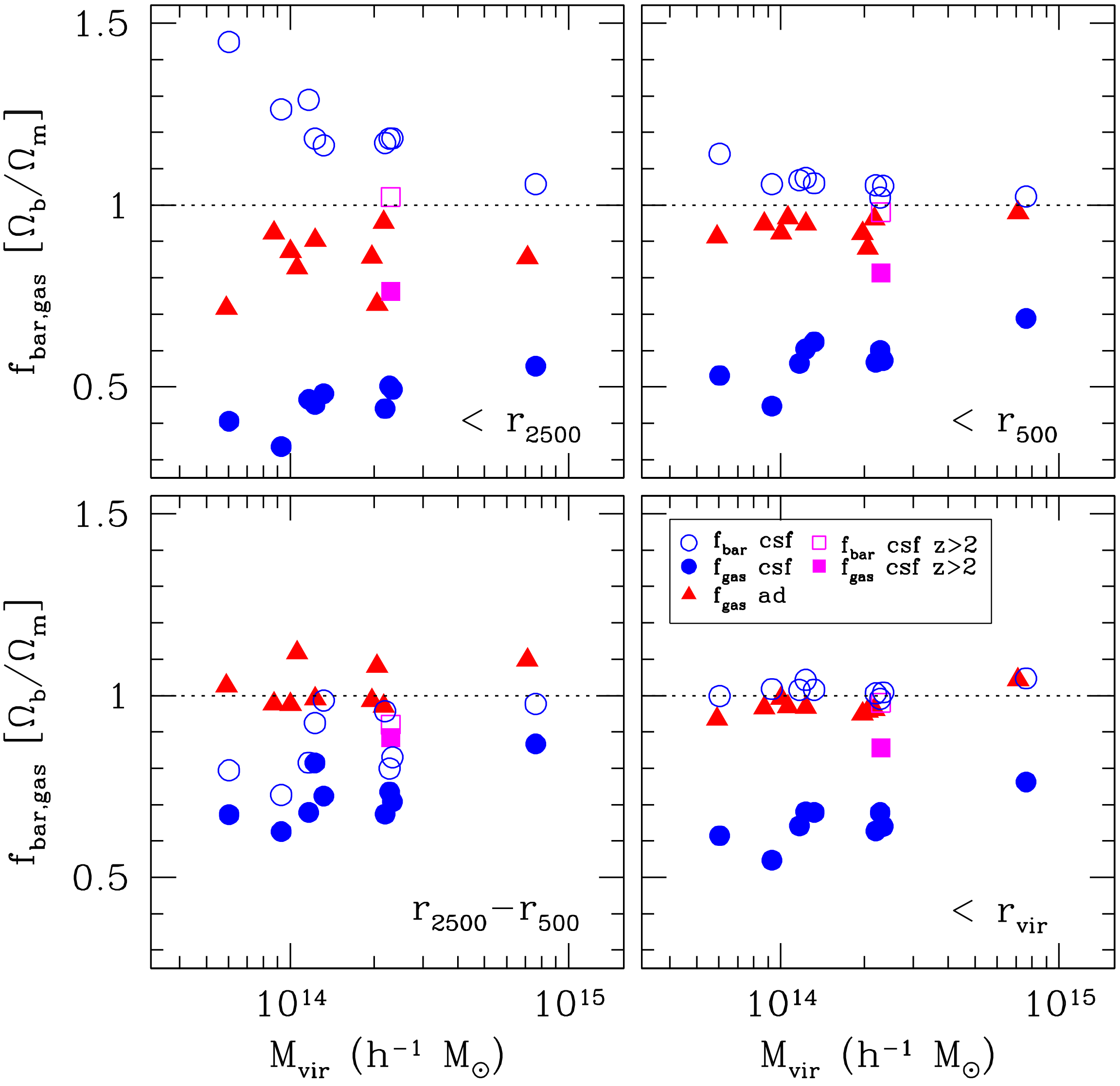

FIG. 4.— The total baryon and gas fractions of individual clusters in units of the universal value within different radii (clockwise from the top left panel: $r < r_{2500}$, $r < r_{500}$, $r < r_{\rm vir}$, in the annulus $r_{2500} - r_{500}$) as a function of the cluster virial mass. *Solid triangles* show the gas fractions in the adiabatic simulations. The *solid circles* show the gas fraction, while *open circles* show the total baryon fraction in the simulations with cooling and star formation. *Solid* and *open squares* show the gas and baryon fractions in the resimulation of CL3, in which cooling was turned off at $z < 2$. Note the systematic trend with mass for the gas fractions in the simulation with cooling.

Figure 3 also shows that the variance around the mean for the cumulative profiles is rather small, especially at large radii. The scatter is somewhat larger at $z = 1$, probably because the clusters are on average less relaxed at the earlier time. However, there is no significant qualitative difference between the profiles at two different epochs.

Figure 4 shows the baryon and gas fractions as a function of the cluster virial mass within r_{2500}, r_{500}, and $r_{\rm vir}$ and within the radial range $[r_{2500} - r_{500}]$. The values of the baryon and gas fractions plotted in this figure are listed in Table 2. The fractions in the adiabatic simulations are marked 'ad', while those in the simulations with cooling and star formation are marked 'csf' (e.g., $f_{\rm gas}^{\rm csf}$). In the table we also provide the mean values and scatter for our cluster sample. Note, however, that these are averages over clusters of different masses and should be interpreted with caution given the trends of the baryon and gas fractions with cluster mass discussed below.

In adiabatic simulations, the baryon fraction appears to be independent of mass for all radial ranges. It is systematically below the universal value by ≈ 15% and ≈ 5% within r_{2500} and r_{500}, respectively. For $r < r_{\rm vir}$, the baryon fraction is within ≈ 5% of the universal value. Note also that in the adiabatic runs, the baryon fraction within the radial range of $r_{2500} - r_{500}$ is close to the universal value on average, even though the cumulative fractions within these radii are systematically below.

In the simulations with cooling and star formation the baryon and gas fractions show (weak) trend with mass. The gas fraction appears to systematically increase with

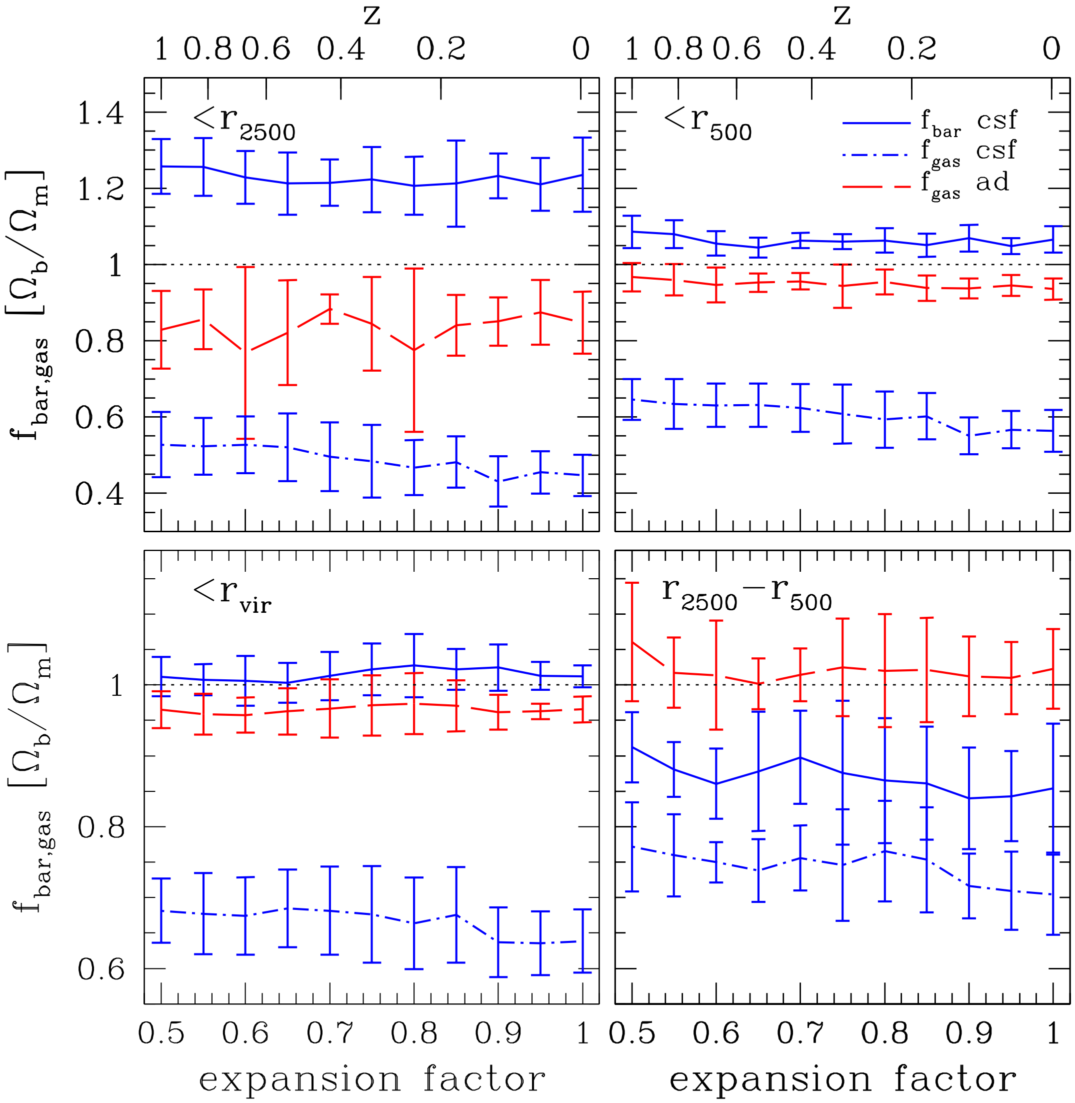

FIG. 5.— Evolution of the baryon and gas fractions within different radii for the eight clusters CL2-CL9 from $z = 1$ to $z = 0$. The radii used are the same as in Fig. 4. The *long-dashed* lines shows the gas fraction in the adiabatic simulations. The *dot-dashed* and *solid* lines show the gas and baryon fraction profiles in the simulation with cooling and star formation. The gas and baryon fractions are normalized to the universal fraction of baryons assumed in the simulations. The figure shows that the evolution of baryon fraction at these redshifts is weak. Note that each cluster at least doubles its mass over this redshift interval.

increasing cluster mass as

$$f_{\rm gas} = 0.2\log(M_{\rm vir}/10^{14}h^{-1}\ {\rm M}_{\odot}) + f_0, \qquad (1)$$

where f_0 is ≈ 0.4, 0.5, 0.6, 0.65 for $r < r_{2500}$, r_{500}, $r_{\rm vir}$, and $r_{2500} - r_{500}$, respectively. The significance of this trend and the value of the slope are uncertain given the small size of the sample. The baryon fraction in the CSF runs is larger than the universal value within r_{500}, but it is within $\approx 2-3\%$ of the universal value within $r_{\rm vir}$. The baryon fraction, $f_{\rm bar}(< r_{\rm vir})$, in these runs is also not biased low like the corresponding fraction in the adiabatic runs but gives the average very close to the universal.

The differential fractions within the radial range $r_{2500} - r_{500}$ behave somewhat differently because they are not affected by the concentration of baryons in the cluster center. In this radial range, the baryon fraction in the adiabatic runs is approximately unbiased. In the CSF runs the baryon fraction is systematically below the universal value but its mass dependence for $M \gtrsim 10^{14}h^{-1}$ M$_{\odot}$ seems to be weaker than for the cumulative fraction within similar radii. In all panels open and solid squares show the baryon and gas fractions for the re-simulation of CL3 with cooling turned off at $z < 2$. As could be expected, the fractions in this case are intermediate between the adiabatic simulation and run with cooling and star formation.

Finally, in Figure 5 we show evolution of the average baryon and gas fractions from $z = 1$ to $z = 0$ within radii shown in the previous figure in the adiabatic and CSF runs of clusters CL2-CL9. The figure shows that the total baryon fractions are quite stable in this redshift interval. This is remarkable given that most clusters undergo at least one major merger at $z < 1$. There is a weak decrease of the gas fraction with time in the CSF simulations, as some of the gas is cooling and is turned into stars. The evolution of $f_{\rm gas}$ is $\approx 10-20\%$ from $z=1$ to $z=0$.

6. COMPARISON TO PREVIOUS WORK

Given the systematic differences in gas fractions in the Santa Barbara cluster comparison (Frenk et al. 1999), it is interesting to compare the results presented in the previous section to other recent studies to assess the current state of affairs. The comparison is relatively straightforward for the adiabatic simulations because all codes should simulate evolution using the same equations of gas and collisionless dynamics. Any differences can therefore be attributed to the difference in the actual numerical scheme. Eke et al. (1998) studied SPH simulations of ten massive clusters formed in the concordance ΛCDM cosmology. They found gas fractions of ≈ 0.99, 0.87, and 0.83 within $3r_{\rm vir}$, $r_{\rm vir}$, and $0.5r_{\rm vir}$ (note that $r_{500}\approx 0.5r_{\rm vir}$), respectively, which evolve only very weakly from $z=1$ to $z=0$. These numbers are similar to those obtained with a number of other SPH codes (Frenk et al. 1999; Bialek et al. 2001; Muanwong et al. 2002). We also find no detectable evolution of baryon fraction in adiabatic simulations over this period of time. However, the gas fractions in our simulations are larger: ≈ 1.00 at $r\gtrsim 3r_{\rm vir}$, and 0.97 ± 0.03 and 0.94 ± 0.03 for $r<r_{\rm vir}$ and $r<r_{500}$. Gas fractions in simulations with the entropy-conserving Gadget code (see Fig. 1) are larger by about 5% than those found by Eke et al. (1998): ≈ 0.92 at $r<r_{\rm vir}$ and ≈ 0.88 if measured within $0.5r_{\rm vir}$. This is consistent with the adiabatic simulations (run with the entropy conserving version of the Gadget) presented in a recent study by Kay et al. (2004), who find the average gas fraction of $\simeq 90\%$ of the universal value within the virial radius. The average gas fraction profile for the adiabatic simulations in their Figure 6 is in good agreement with the Gadget simulations presented here.

The studies of baryon fraction in simulations with cooling and star formation are fewer and the source of the differences is usually not as clear, because it can be attributed both to a different implementation of these processes and to the difference between numerical gasdynamics schemes. Muanwong et al. (2002) compared the baryon and gas fractions as a function of cluster virial mass in adiabatic simulations and re-simulations in which gas was allowed to cool or was pre-heated (see their Fig. 3). For the mass range of our cluster sample, in simulations with cooling Muanwong et al. (2002) obtain baryon fractions of $\approx 0.85-0.9$ of the universal value within the virial radius. This is slightly larger than in their adiabatic simulations, but is considerably lower than in our simulations with cooling and star formation (1.02 ± 0.02, see Table 2). Valdarnini (2003) compares gas fractions in in TREESPH simulations that include cooling and star formation to the observational estimates of Arnaud & Evrard (1999) and finds a reasonable agreement. Valdarnini (2003) also finds indications of a trend of increasing $f_{\rm gas}$ with increasing cluster mass similar to the trend we find in our simulations. The actual gas fractions in this study are, however, somewhat lower than our values, which may be due to a lower assumed universal baryon fractions ($\Omega_{\rm b}h^2=0.015-0.019$) compared to the value assumed in this study. Kay et al. (2004) analyze a sample of 15 clusters simulated using the entropy-conserving Gadget code with cooling, star formation, and feedback. Their average gas fraction profile for these simulations agree well with the gas fraction profile of our small-mass clusters (CL2-CL9), but is considerably lower than that for our Coma-size cluster (CL1). Most recently, Ettori et al. (2004) presented a similar analysis for the simulations with cooling and star formation of a statistical sample of clusters simulated with the entropy-conserving version of the Gadget code. These authors, quote total baryon fractions of $f_{\rm bar}(<r_{\rm vir})\approx 0.93-0.95$ of the universal value in their simulations. This is closer to the values in our simulations. Their gas fractions are $0.75-0.8$ — higher than in our clusters due to a different implementation of cooling and star formation.

These comparisons and the comparison with the Gadget code presented in § 3 indicate that there are still systematic differences between the eulerian and SPH codes, with the latter predicting systematically smaller baryon fractions. The difference appears to be the smallest when eulerian simulations are compared to the entropy-conserving Gadget SPH code.

7. DISCUSSION AND CONCLUSIONS

We have presented results of the analysis of baryon and gas fractions in the high-resolution simulations of nine galaxy clusters formed in the concordance ΛCDM cosmology. The clusters span the range of virial masses from $M_{\rm vir}=6\times10^{13}$ to $8\times10^{14}h^{-1}$ $\rm M_\odot$ and have *not* been selected to be in the highly relaxed state at the present epoch. We study the effects of cooling and star formation by comparing simulations of individual clusters done with and without these processes included.

We show that radiative cooling of gas and subsequent star formation significantly modify distribution of baryons within the virial radii of galaxy clusters in our simulations. The effect is twofold. First, cooling results in a condensation of gas and dark matter in the centers of halos (Zeldovich et al. 1980; Barnes & White 1984; Blumenthal et al. 1986; Jesseit et al. 2002; Gnedin et al. 2004). As the gas cools in the cluster progenitor, the baryons condense near the cluster center (the central cluster galaxy). The condensing gas has to be replaced by the gas from larger radii. The net result is that the baryon fraction is affected at radii up to $\sim r_{\rm vir}$. For example, Figure 3 shows that the cumulative baryon fraction in the simulations with cooling is systematically higher than in the adiabatic runs at $r\lesssim 1.5r_{\rm vir}$ with the difference of $\approx 5\%$ at $r_{\rm vir}$. Dissipation thus allows clusters to collect a larger fraction of baryons within their virialized region. Remarkably, in these simulations baryon fraction within the virial radius is very close (to $\approx 2-3\%$) to the universal value. Note that for the differential baryon fraction, $f_{\rm bar}(r)$, the effect at large radii is opposite. In the simulations with cooling $f_{\rm bar}(r)$ is systematically smaller than in the adiabatic simulations at $r>0.1r_{\rm vir}$. The overall increase in the cumulative baryon fraction is therefore driven by the baryons in the central cluster galaxy.

Second, a fraction of gas is converted into collisionless stellar component. The ratio of stellar to gas mass depends on the distance to the cluster center. In cluster cores ($r\lesssim 0.2r_{\rm vir}$) stellar fraction dominates the baryon budget, $f_*\gtrsim 50-70\%$ depending on cluster mass. At larger radii most baryons remain in the form of gas with

TABLE 2
Baryon and gas fractions in cluster simulations at the present day epoch

Cluster	$r < r_{2500}$			$r < r_{500}$			$r_{2500} - r_{500}$			$r < r_{\rm vir}$		
	$f_{\rm bar}^{\rm ad}$	$f_{\rm gas}^{\rm csf}$	$f_{\rm bar}^{\rm csf}$	$f_{\rm bar}^{\rm ad}$	$f_{\rm gas}^{\rm csf}$	$f_{\rm bar}^{\rm csf}$	$f_{\rm bar}^{\rm ad}$	$f_{\rm gas}^{\rm csf}$	$f_{\rm bar}^{\rm csf}$	$f_{\rm bar}^{\rm ad}$	$f_{\rm gas}^{\rm csf}$	$f_{\rm bar}^{\rm csf}$
CL1	0.86	0.56	1.06	0.98	0.69	1.02	1.10	0.87	0.98	1.04	0.76	1.05
CL2	0.73	0.44	1.17	0.88	0.57	1.05	1.08	0.67	0.79	0.96	0.63	1.01
CL3	0.95	0.49	1.18	0.96	0.57	1.05	0.97	0.71	0.83	0.96	0.64	1.01
CL4	0.86	0.50	1.18	0.92	0.60	1.02	0.99	0.74	0.80	0.95	0.68	0.99
CL5	0.90	0.48	1.16	0.95	0.62	1.06	0.99	0.72	0.99	0.97	0.68	1.02
CL6	0.92	0.34	1.26	0.95	0.45	1.06	0.98	0.63	0.73	0.97	0.55	1.02
CL7	0.87	0.45	1.18	0.92	0.60	1.08	0.98	0.82	0.92	0.99	0.68	1.04
CL8	0.83	0.47	1.29	0.97	0.56	1.07	1.12	0.68	0.82	0.97	0.64	1.02
CL9	0.72	0.41	1.45	0.91	0.53	1.14	1.03	0.67	0.79	0.94	0.61	1.00
mean	0.85	0.46	1.22	0.94	0.58	1.06	1.02	0.72	0.87	0.97	0.65	1.02
scatter	0.08	0.06	0.11	0.03	0.07	0.03	0.06	0.08	0.09	0.03	0.06	0.02

$f_* \lesssim 10-20\%$ at $r > r_{2500}$. The collisionless dynamics of stars is different from the dynamics of gas in detail. For example, the gas in a galaxy or a group can be ram-pressure stripped and deposited at larger radii, while the stars can sink to the center via dynamical friction. During mergers, the gas is shock-heated, while stellar particles relax via the violent relaxation. When stars are formed, a smaller fraction of baryons is subject to strong shocks that may prevent accretion of some of the gas into the inner regions of clusters. The differences in dynamics can modify the total baryon fraction profile and the ratio of stellar to gas mass at different radii.

To gauge how robust are the predictions of numerical simulations, we have compared the gas fraction profiles for the eight clusters in our sample, simulated in the adiabatic regime with the entropy-conserving Gadget and the ART codes. The profiles in the two sets of simulations agree to better than $\approx 3\%$ outside the cluster core ($r/r_{\rm vir} \gtrsim 0.2$), but differ by up to 10% at small radii. The main difference is thus in the cluster core where the gas profiles in the Gadget simulations are more centrally concentrated and the gas fractions are correspondingly larger than in the ART runs. This is reflected in systematic difference in the cumulative baryon fraction profiles at $r \gtrsim r_{2500}$: 95% in the ART runs compared to 92% in the Gadget simulations. The discrepancy is smaller than the difference in gas fractions of $\approx 10\%$ between SPH and eulerian codes in the Santa Barbara comparison project (Frenk et al. 1999). Nevertheless, it is systematic (similar for all eight compared clusters) and one has to keep it in mind when interpreting or using results of numerical simulations. Note also that this comparison was done for the simplest case of the adiabatic gas dynamics. The differences in baryon and gas fractions are likely to be larger when cooling and star formation are included. We discussed how our results compare with some of the recent simulation results in the previous section. We also plan to compare our results with the results of the Gadget simulations with cooling and star formation in the near future.

One should note that cluster simulations may suffer from the "overcooling problem." Indeed, the fraction of baryons in the cold gas and stars within the virial radius of clusters at $z = 0$ in our simulations is in the range $\sim 0.25 - 0.35$, at least a factor of two higher than observational measurements for the systems of the mass range we consider (Lin et al. 2004). Such high fractions of baryons in condensed cold gas or stars are generic results of cosmological simulations, although specific numerical values vary (e.g., Suginohara & Ostriker 1998; Lewis et al. 2000; Pearce et al. 2000; Davé et al. 2002; Ettori et al. 2004). We have done an extensive convergence study, varying the numerical resolution, implementation of cooling, star formation and stellar feedback, and assumed baryon fraction. However, we have not been able to reduce stellar fractions considerably below the values presented in this study.

Note that Motl et al. (2004) have recently presented eulerian AMR simulations of two massive galaxy clusters ($M_{\rm vir} \approx 2 \times 10^{15} h^{-1}$ M$_\odot$) with the fraction of cold ($T < 15000$ K) condensed gas of $\approx 10\%$. It is not yet clear whether this represents a discrepancy with our results. The number of simulated massive clusters is clearly small. At the same time, the two simulated clusters analyzed by Motl et al. (2004) have mass a factor of two larger than our most massive cluster. If the trend of increasing $f_{\rm gas}$ (and correspondingly decreasing f_*) with increasing cluster mass (see Fig. 4) continues to larger masses, equation (1) gives $f_{\rm gas} \approx 90\%$ for the cluster masses considered by Motl et al. (2004), in agreement with their results.

The efficient dissipation and persistence of late star formation may indicate that some mechanism suppressing gas cooling is needed. The problem appears to be in the central brightest cluster galaxy, which contains a larger fraction of cluster mass than is measured in observations. The rest of the cluster galaxies have stellar masses in reasonable agreement with observations (Nagai & Kravtsov, in preparation). The overcooling problem in simulations may thus be related to the puzzling absence of cold gas in the observed cluster cores (e.g., Peterson et al. 2003). At the same time, some fraction of cluster stellar mass in low-surface brightness intracluster component may be missed in observations, which could reduce the apparent discrepancy of observed f_* with the simulation results (e.g., Gonzalez et al. 2004; Lin & Mohr 2004). For example, baryon fractions within virial radii of rich clusters do not seem to add up to the universal value from the WMAP observations (Spergel et al. 2003), as they do in both adiabatic and dissipative simulations (see, e.g., Ettori 2003).

Interestingly, gas fractions measured in our CSF simulations are consistent with the observed gas fractions in clusters (Evrard 1997; Mohr et al. 1999; Arnaud & Evrard 1999; Roussel et al. 2000). For example, Evrard (1997) presents estimates of the gas fractions within radius of r_{500} for a sample of galaxy clusters spanning a wide range of the ICM temperatures. The gas fractions vary from ~ 50 to 85% of the universal value (assuming $\Omega_{\rm b} = 0.043$ and $h = 0.7$) in rough agreement with our results. The values of gas fraction in units of the universal value, $f_{\rm bar} = 0.143$, estimated from the virial scaling relations by Mohr et al. (1999) are[7] $f_{\rm gas}(< r_{500})/f_{\rm bar} \sim 0.5 - 0.7$ for clusters with temperatures of $T_X \approx 4$ keV and $f_{\rm gas}(< r_{500})/f_{\rm bar} \sim 0.65 - 0.85$ for $T_X \approx 8$ keV. The latter is also consistent with the measurements based on the SZ cluster observations and X-ray temperature of $T_X \gtrsim 5$ keV clusters (Grego et al. 2001). More recently, Sanderson et al. (2003) presented analysis of gas fractions in a large sample of clusters spanning a wide range of masses. The resulting values of gas fraction depend on the assumptions made, but overall the values are larger than in our simulations. For instance the mean gas fraction for their clusters is 0.13 ± 0.01 or in units of our universal baryon fraction 91%. Similarly to our simulated clusters, the real clusters in their sample show gas fractions monotonically increasing with cluster-centric radius. Sanderson et al. (2003) also found a trend of increasing gas fraction with increasing cluster mass (see also Mohr et al. 1999; Arnaud & Evrard 1999) roughly consistent with the trend for our sample of simulated clusters (see Figure 4 and eq. [1]). A caveat is that gas fractions in these studies have been estimated either using the β-model fits to the data or virial scaling relations rather than directly measuring gas and total mass within r_{500}.

We also note that Bryan (2000) used observational data compiled from the literature to argue that there is a trend of decreasing stellar mass fractions with increasing cluster mass: $f_* = 0.042(T/10\,{\rm keV})^{-0.35}$, where T is the emission-weighted ICM temperature. Given that $T \propto M^{2/3}$ according to the expected virial scaling, the corresponding scaling as a function of cluster mass, $f_* \propto M^{-0.23}$, and its normalization are in good agreement with our simulations.

More recently, high sensitivity of the *Chandra* and *XMM-Newton* satellites allowed reliable measurements of temperature profiles and direct estimates of gas fractions from the full hydrostatic equilibrium analyses. For instance, Allen et al. (2004) present gas fraction profiles at $r < r_{2500}$ for a sample of 26 massive clusters ($T_X > 5$ keV) at different redshifts ($0 < z < 1$). They quote gas fractions $f_{\rm gas}(< r_{2500}) \approx 0.12$ for the cosmology adopted in our study. The corresponding gas fraction for the massive cluster (CL1) in our study is 0.08. This lower value may be due to the fact that most of the clusters in the Allen et al. (2004) are more massive than CL1[8] or may indicate overcooling in simulations. It may also be simply due to the higher value of the universal baryon fraction in the real Universe. For example, if we use the value preferred by the WMAP data (Spergel et al. 2003), $\Omega_{\rm b}/\Omega_{\rm m} \simeq 0.17$, the CL1 gas fraction in units of the universal value agrees with the observed values in Allen et al. (2004). A larger sample of massive simulated clusters or comparison with a sample of lower mass clusters is needed for a reliable conclusion.

The results presented in this paper have a number of implications for the analyses that use clusters to obtain cosmological constraints. First of all, our results show that cooling changes the cumulative baryon and gas fractions appreciably even at the virial radius. Within the inner regions of clusters ($r \lesssim r_{2500}$) the difference between cooling and adiabatic simulations of the same cluster can be as large as $\sim 20 - 40\%$. The effects are smaller for more massive clusters or if the real clusters have lower fraction of condensed baryons than clusters in our simulations. However, even for the simulation in which stellar fraction is twice smaller ($f_* \approx 0.15$ in the re-simulation of CL3 with cooling turned off at $z < 2$) we find 20% change in gas fraction and $\approx 7\%$ change in the total baryon fraction within r_{2500} compared to the adiabatic run. These differences are still large if baryon fractions are to be used for precision cosmological constraints. Our analysis also shows that in simulations with cooling the total baryon fraction can either be larger or smaller than the universal fraction depending on the chosen radius and cluster mass. Therefore, there is no single universal correction for converting the measured baryon fraction to the universal value. These results suggest that care should be taken in observational analyses to estimate baryon fractions, and the systematic errors are likely mitigated if the measurements are made at radii least affected by cooling and least sensitive to the uncertain contribution of stars to the baryon budget.

Cooling and star formation decrease the fraction of hot intracluster gas within the virial radius of the cluster. This decrease may affect the Sunyaev-Zeldovich (SZ) fluxes and their relation to cluster mass. Upcoming large SZ surveys will have a large fraction of objects with masses of a few$\times 10^{14}$ $M_{\odot}$. In such clusters star formation can decrease the gas fraction by $\sim 20 - 40\%$ depending on cluster mass. The trend of gas fraction with mass will also modify the slope of the relation between SZ flux and cluster mass. The trend is weak but may need to be taken into account to ensure accurate cosmological constraints.

Given the importance of these issues for the use of clusters as cosmological probes, further effort from both theorists and observers is needed to evaluate effects of cooling and to make robust measurements of baryon fractions (gas+stars) in clusters. Theoretically, it is important to simulate larger samples of clusters over a wide range of masses and with high resolution and to investigate the role of various processes (such as, for example, thermal conduction and AGN feedback; e.g., Bruggen et al. 2005) in suppressing cooling and star formation in cluster cores, as well as processes such as helium segregation which can affect cluster baryon fractions (Qin & Wu 2000; Chuzhoy & Loeb 2004). However, it is even more important to first understand how large is the difference between the stellar fractions in observed and simulated clusters. If the fraction of the diffuse intracluster stars is as large as 50% (Gonzalez et al. 2004; Lin & Mohr 2004, see however Zibetti et al. 2005), f_* in our simulations actually agrees with observations. Careful observational calibration of stellar masses in clusters (see, e.g., Voevodkin et al. 2002; Lin et al. 2004) using deep images in red or infrared bands would go a long way in clarifying this issue.

---

[7] We have calculated the gas fractions for $h = 0.7$.

[8] There are some clusters in their sample that have $f_{\rm gas}(< r_{2500}) < 0.1$

We would like to thank Gustavo Yepes for providing us the gas fraction profiles of the clusters simulated with the Gadget code and useful discussions, and Volker Springel for making the entropy-conserving version of Gadget available. This project was supported by the National Science Foundation (NSF) under grants No. AST-0206216 and AST-0239759, by NASA through grant NAG5-13274, and by the Kavli Institute for Cosmological Physics at the University of Chicago. D.N. is supported by the NASA Graduate Student Researchers Program and by NASA LTSA grant NAG5–7986. AV is supported by the NASA grant NAG5-9217 and contract NAS8-39073. The cosmological simulations used in this study were performed on the IBM RS/6000 SP4 system (`copper`) at the National Center for Supercomputing Applications (NCSA).

REFERENCES

Allen, S. W., Schmidt, R. W., Ebeling, H., Fabian, A. C., & van Speybroeck, L. 2004, MNRAS, 353, 457
Allen, S. W., Schmidt, R. W., & Fabian, A. C. 2002, MNRAS, 334, L11
Anninos, P. & Norman, M. L. 1996, ApJ, 459, 12
Arnaud, M. & Evrard, A. E. 1999, MNRAS, 305, 631
Ascasibar, Y., Yepes, G., Müller, V., & Gottlöber, S. 2003, MNRAS, 346, 731
Barnes, J. & White, S. D. M. 1984, MNRAS, 211, 753
Bialek, J. J., Evrard, A. E., & Mohr, J. J. 2001, ApJ, 555, 597
Blumenthal, G. R., Faber, S. M., Flores, R., & Primack, J. R. 1986, ApJ, 301, 27
Borgani, S., Governato, F., Wadsley, J., Menci, N., Tozzi, P., Quinn, T., Stadel, J., & Lake, G. 2002, MNRAS, 336, 409
Bruggen, M., Ruszkowski, M., & Hallman, E. 2005, ApJ submitted (astro-ph/0501175)
Bryan, G. L. 2000, ApJ, 544, L1
Chen, G. & Ratra, B. 2004, ApJ, 612, L1
Chuzhoy, L. & Loeb, A. 2004, MNRAS, 349, L13
Davé, R., Katz, N., & Weinberg, D. H. 2002, ApJ, 579, 23
Eke, V. R., Navarro, J. F., & Frenk, C. S. 1998, ApJ, 503, 569
Ettori, S. 2003, MNRAS, 344, L13
Ettori, S., Borgani, S., Moscardini, L., Murante, G., Tozzi, P., Diaferio, A., Dolag, K., Springel, V., Tormen, G., & Tornatore, L. 2004, MNRAS, 354, 111
Evrard, A. E. 1990, ApJ, 363, 349
—. 1997, MNRAS, 292, 289
Ferland, G. J., Korista, K. T., Verner, D. A., Ferguson, J. W., Kingdon, J. B., & Verner, E. M. 1998, PASP, 110, 761
Frenk, C. S., White, S. D. M., Bode, P., Bond, J. R., Bryan, G. L., Cen, R., Couchman, H. M. P., Evrard, A. E., Gnedin, N., Jenkins, A., Khokhlov, A. M., Klypin, A., Navarro, J. F., Norman, M. L., Ostriker, J. P., Owen, J. M., Pearce, F. R., Pen, U.-L., Steinmetz, M., Thomas, P. A., Villumsen, J. V., Wadsley, J. W., Warren, M. S., Xu, G., & Yepes, G. 1999, ApJ, 525, 554
Gnedin, O. Y., Kravtsov, A. V., Klypin, A. A., & Nagai, D. 2004, ApJ, 616, 16
Gonzalez, A. H., Zabludoff, A. I., & Zaritsky, D. 2004, ApJ submitted (`astro-ph/0406244`)
Grego, L., Carlstrom, J. E., Reese, E. D., Holder, G. P., Holzapfel, W. L., Joy, M. K., Mohr, J. J., & Patel, S. 2001, ApJ, 552, 2
Haardt, F. & Madau, P. 1996, ApJ, 461, 20
Hartmann, L. 2002, ApJ, 578, 914
Jesseit, R., Naab, T., & Burkert, A. 2002, ApJ, 571, L89
Jungwiert, B., Combes, F., & Palouš, J. 2001, A&A, 376, 85
Kay, S. T., Thomas, P. A., Jenkins, A., & Pearce, F. R. 2004, MNRAS, 355, 1091
Kay, S. T., Thomas, P. A., & Theuns, T. 2003, MNRAS, 343, 608
Kennicutt, R. C. 1998, ApJ, 498, 541
Klypin, A., Kravtsov, A. V., Bullock, J. S., & Primack, J. R. 2001, ApJ, 554, 903
Kravtsov, A. V. 1999, PhD thesis, New Mexico State University
Kravtsov, A. V., Klypin, A., & Hoffman, Y. 2002, ApJ, 571, 563
Lewis, G. F., Babul, A., Katz, N., Quinn, T., Hernquist, L., & Weinberg, D. H. 2000, ApJ, 536, 623
Lin, Y. & Mohr, J. J. 2004, ApJsubmitted (`astro-ph/0408557`)
Lin, Y., Mohr, J. J., & Stanford, S. A. 2004, ApJ, 610, 745
Lubin, L. M., Cen, R., Bahcall, N. A., & Ostriker, J. P. 1996, ApJ, 460, 10
Metzler, C. A. & Evrard, A. E. 1994, ApJ, 437, 564
Miller, G. E. & Scalo, J. M. 1979, ApJS, 41, 513
Mohr, J. J., Mathiesen, B., & Evrard, A. E. 1999, ApJ, 517, 627
Motl, P. M., Burns, J. O., Loken, C., Norman, M. L., & Bryan, G. 2004, ApJ, 606, 635
Muanwong, O., Thomas, P. A., Kay, S. T., & Pearce, F. R. 2002, MNRAS, 336, 527
Navarro, J. F., Frenk, C. S., & White, S. D. M. 1995, MNRAS, 275, 720
Pearce, F. R., Thomas, P. A., Couchman, H. M. P., & Edge, A. C. 2000, MNRAS, 317, 1029
Pen, U. 1997, New Astronomy, 2, 309
Peterson, J. R., Kahn, S. M., Paerels, F. B. S., Kaastra, J. S., Tamura, T., Bleeker, J. A. M., Ferrigno, C., & Jernigan, J. G. 2003, ApJ, 590, 207
Qin, B. & Wu, X. 2000, ApJ, 529, L1
Roussel, H., Sadat, R., & Blanchard, A. 2000, A&A, 361, 429
Sanderson, A. J. R., Ponman, T. J., Finoguenov, A., Lloyd-Davies, E. J., & Markevitch, M. 2003, MNRAS, 340, 989
Sasaki, S. 1996, PASJ, 48, L119
Spergel, D. N., Verde, L., Peiris, H. V., Komatsu, E., Nolta, M. R., Bennett, C. L., Halpern, M., Hinshaw, G., Jarosik, N., Kogut, A., Limon, M., Meyer, S. S., Page, L., Tucker, G. S., Weiland, J. L., Wollack, E., & Wright, E. L. 2003, ApJS, 148, 175
Springel, V. & Hernquist, L. 2002, MNRAS, 333, 649
Springel, V., Yoshida, N., & White, S. D. M. 2001, New Astronomy, 6, 79
Suginohara, T. & Ostriker, J. P. 1998, ApJ, 507, 16
Valdarnini, R. 2003, MNRAS, 339, 1117
Vikhlinin, A., Voevodkin, A., Mullis, C. R., VanSpeybroeck, L., Quintana, H., McNamara, B. R., Gioia, I., Hornstrup, A., Henry, J. P., Forman, W. R., & Jones, C. 2003, ApJ, 590, 15
Voevodkin, A. & Vikhlinin, A. 2004, ApJ, 601, 610
Voevodkin, A. A., Vikhlinin, A. A., & Pavlinsky, M. N. 2002, Astronomy Letters, 28, 366
White, S. D. M., Navarro, J. F., Evrard, A. E., & Frenk, C. S. 1993, Nature, 366, 429
Woosley, S. E. & Weaver, T. A. 1995, ApJS, 101, 181
Zeldovich, Y. B., Klypin, A. A., Khlopov, M. Y., & Chechetkin, V. M. 1980, Soviet J. Nucl. Phys., 31, 664
Zibetti, S., White, S., Schneider, D. P., & Brinkmann, J. 2005, MNRAS in press (astro-ph/0501194)